

A spin-adapted Density Matrix Renormalization Group algorithm for quantum chemistry

Sandeep Sharma and Garnet Kin-Lic Chan*

Department of Chemistry and Chemical Biology, Cornell University, Ithaca NY14853

We extend the spin-adapted density matrix renormalization group (DMRG) algorithm of McCulloch and Gulacsi [1] to quantum chemical Hamiltonians. This involves two key modifications to the non-spin-adapted DMRG algorithm: the use of a quasi-density matrix to ensure that the renormalised DMRG states are eigenvalues of \hat{S}^2 , and the use of the Wigner-Eckart theorem to greatly reduce the overall storage and computational cost. We argue that the advantages of the spin-adapted DMRG algorithm are greatest for low spin states. Consequently, we also implement the singlet-embedding strategy of Nishino *et al* [2] which allows us to target high spin states as a component of a mixed system which is overall held in a singlet state. We evaluate our algorithm on benchmark calculations on the Fe_2S_2 and Cr_2 transition metal systems. By calculating the full spin ladder of Fe_2S_2 , we show that the spin-adapted DMRG algorithm can target very closely spaced spin states. In addition, our calculations of Cr_2 demonstrate that the spin-adapted algorithm requires only roughly half the number of renormalised DMRG states as the non-spin-adapted algorithm to obtain the same accuracy in the energy, thus yielding up to an order of magnitude increase in computational efficiency.

I. INTRODUCTION

Since its introduction by White [3, 4] and its first application to quantum chemical systems [5], the density matrix renormalization group (DMRG) has been applied to a wide variety of problems in quantum chemistry [6–11]. After early attempts to use the DMRG as a full configuration interaction (FCI) method for small molecules [7, 10, 12–14], it was recognised that DMRG is best used to describe non-dynamical correlation in active spaces. The DMRG algorithm exhibits a polynomial cost scaling $O(k^3M^3) + O(k^4M^2)$, where k is the number of active space orbitals, and M is the number of renormalised many-body states which determine the accuracy of the method. In non 1-D systems, the number of states M required to obtain a given error (relative to the FCI energy in the active space) depends on the correlation length of the system with the orbitals mapped onto an artificial 1-D lattice, and this can increase quite rapidly with k . In addition, the shape of the orbitals and the order in which they are arranged can drastically affect the convergence of the DMRG [15, 16]. Nonetheless, many examples have demonstrated that in practical applications, the DMRG describes active space correlations to high accuracy, for orbital spaces beyond the reach of complete active space non-dynamical correlation methods.

Transition metal chemistry typically involves partially filled d orbitals and is a rich source of difficult active space correlation problems. Increasing effort in recent times has been devoted to applications of the DMRG to transition metal chemistry [8, 11, 17–21]. Here, the ability to correctly handle spin symmetry is an important asset. This is because the large number of unpaired electrons often leads to many low lying spin states in a very narrow energy window. These can only be efficiently resolved by targetting a specific spin sector. In addition, of course, the correct use of spin symmetry offers the promise of computational efficiency gains.

Spin symmetry is associated with the non-Abelian $\text{SU}(2)$ Lie group. Spin adaptation in the DMRG can be achieved by working with states and operators (multiplets and irreducible tensor operators, respectively) that transform as irreducible representations of $\text{SU}(2)$. This formulation resembles quantum chemistry approaches to spin adaptation which work directly in the configuration state function basis, rather than alternatives based on the symmetric [22, 23] or unitary groups [24–26]. The first DMRG algorithm to exploit non-Abelian spin symmetry was the interaction-round-a-face DMRG (IRF-DMRG) introduced by Sierra *et al.* [27, 28]. McCulloch *et al.* [1, 29, 30] later proposed a highly efficient implementation of spin-adapted DMRG. Their algorithm relied on two important ingredients. The first was the use of a quasi-density matrix to determine the renormalized DMRG basis. In general, the density matrix of a subsystem does not commute with the total spin operator of the subsystem, and thus the usual DMRG prescription, to use the density matrix eigenvectors as the many-body basis, is incompatible with spin adaptation. McCulloch *et al.* showed that the best states to retain in the decimation step of the DMRG are eigenvectors of a *quasi-density* matrix which commutes with the \hat{S}^2 operator. The second contribution was the use of the Wigner-Eckart theorem to efficiently store and compute matrix elements of irreducible tensor operators. This leads to significant improvements

* Corresponding author. Electronic mail: gc238@cornell.edu



FIG. 1: The one-dimensional arrangement of orbitals on a lattice and the subdivision into blocks. In the forward sweep the left block is termed the system block and the right block is termed the environment block and the reverse is true in the backward sweep. At each sweep iteration the system block increases in size by one orbital.

in the performance of DMRG. In this work, we closely follow McCulloch *et al.* and extend their algorithm to deal with the more complicated Hamiltonians in quantum chemical systems. We note that earlier work on spin-adapted DMRG in the context of quantum chemistry was carried out by Zgid *et al.* [10]. Zgid *et al.* used quasi-density matrices to ensure the proper spin symmetry of the renormalised states but did not take advantage of the Wigner-Eckart theorem. As we will show, while the Wigner-Eckart formulation complicates the implementation of the DMRG algorithm significantly, it also results in substantial performance gains.

We start with a brief summary of the DMRG algorithm in Section II. We assume that the reader has some familiarity with the DMRG algorithm as described in various articles [7, 11, 31, 32], thus we focus mainly on aspects of the DMRG that will be modified when spin adaptation is introduced. In section III we describe in some detail our implementation of spin adaptation in DMRG. We review concepts related to spin symmetry, such as the Wigner-Eckart theorem, Clebsch-Gordan coefficients, 6- j coefficients, and 9- j coefficients, although the reader will benefit from more detailed expositions, for example in Refs. [33, 34]. In section IV we present our analysis of the main computational differences between the spin-adapted and non-spin-adapted algorithms and describe the singlet embedding approach to high spin states. Finally in Section V we present some sample calculations on transition metal systems, that demonstrate the advantages of using the spin-adapted DMRG algorithm. The appendices summarise some useful relations between the various Clebsch-Gordan coefficients, and describes spin adaptation in the matrix product state language.

II. A SUMMARY OF THE DMRG ALGORITHM

The basic DMRG algorithm consists of a set of sweeps over the k spatial orbitals of the problem. We imagine these orbitals to be arranged as a one dimensional lattice of sites. At every step of the algorithm, the lattice is conceptually divided into four parts: a left block \mathcal{L} consisting of sites $1 \dots p-1$, a left dot \bullet_l , consisting of site p , a right dot \bullet_r consisting of site $p+1$, and a right block \mathcal{R} consisting of sites $p+2 \dots k$ (see Figure 1). In the forward sweeps, the orbital index p increases from $2 \dots k-2$, and block \mathcal{L} increases in size to cover the lattice, while block \mathcal{R} shrinks. During the backwards sweeps, the index p iterates backwards from $k-2 \dots 2$, and block \mathcal{R} increases in size to cover the lattice, while block \mathcal{L} shrinks. When it is necessary to refer to blocks at different sweep iterations, we will use additional subscripts to indicate the sites spanned by block. For example, in successive iterations in a forward sweep, the two \mathcal{L} blocks would be \mathcal{L}_{p-1} (sites $1 \dots p-1$) and \mathcal{L}_p (sites $1 \dots p$), and the two left dots would be \bullet_p and \bullet_{p+1} . We refer to the set of computations performed at each value of index p as a sweep iteration; a sweep thus contains $k-4$ sweep iterations. In total, the full calculation consists of multiple forwards and backwards sweeps (each containing multiple sweep iterations) until convergence in the energy is observed.

Blocks \mathcal{L} and \mathcal{R} are each associated with M many body states, denoted by $\{|l\rangle\}$ and $\{|r\rangle\}$ respectively, where the state labels range from $l, r = 1 \dots M$. (If we need to be more specific about the nature of the block we will attach subscripts e.g. block \mathcal{L}_{p-1} contains states $|l_{p-1}\rangle$.) In successive sweeps of the DMRG algorithm, these many body spaces are variationally improved. The left and right dots are associated with the complete Fock spaces of their respective orbitals $\{|n_l\rangle\}$, $\{|n_r\rangle\}$ respectively, where $|n\rangle \in \{|-\rangle, |\alpha\rangle, |\beta\rangle, |\alpha\beta\rangle\}$.

During the calculation we wish to calculate observables, that is, expectation values of operators such as the Hamiltonian. In general such operators can be expressed as (sums of) products of operators partitioned between the four blocks. For example, a two particle density matrix element operator $a_i^\dagger a_j^\dagger a_k a_l$ is partitioned amongst the blocks depending on the values of the indices i, j, k, l . (Note we use the indices to specify spin orbitals; later while describing the spin-adapted algorithm the indices will be used to specify spatial orbitals. The distinction will be clear from the context). The Hamiltonian across the whole lattice involves sums of the density matrix element operators, and can thus be partitioned in multiple ways into operators on each of the different blocks.

$$\hat{H} = \sum_{ij} t_{ij} a_i^\dagger a_j + \frac{1}{2} \sum_{ijkl} v_{ijkl} a_i^\dagger a_j^\dagger a_k a_l \quad (1)$$

TABLE I: Definition of the operators used in the DMRG algorithm. Here the indices are spin indices not spatial indices.

Operator	Definition
\hat{A}_{ij}	$a_i^\dagger a_j^\dagger$
\hat{B}_{ij}	$a_i^\dagger a_j$
\hat{R}_i	$\sum_j t_{ij} a_j + \sum_{jkl} v_{ijkl} a_j^\dagger a_k a_l$
\hat{P}_{ij}	$\sum_{kl} v_{ijkl} a_k a_l$
\hat{Q}_{ij}	$\sum_{kl} (v_{ikjl} - v_{iklj}) a_k^\dagger a_l$

The following set of operators and their adjoints, defined in Table II, provides an efficient partitioning: $\hat{1}, a_i, \hat{A}_{ij}, \hat{B}_{ij}, \hat{R}_i, \hat{P}_{ij}, \hat{Q}_{ij}, \hat{H}$ [35]. $\hat{R}_i, \hat{P}_{ij}, \hat{Q}_{ij}$ are known as complementary operators, and their definitions involve the one- and two-electron integrals.

The computations in a sweep iteration consists of manipulations of states and operators in the spaces associated with the four blocks $\mathcal{L}, \bullet_l, \bullet_r, \mathcal{R}$. These computations are divided into three steps blocking, wavefunction solution, and renormalization and decimation. We now describe these computations in the context of a forward sweep.

Blocking — This consists, conceptually, of adding the left dot to the left block and the right dot to the right block to form blocks $\mathcal{A} = \mathcal{L}\bullet_l$ and $\mathcal{B} = \bullet_r\mathcal{R}$, respectively. Blocks \mathcal{A} and \mathcal{B} are each associated with many body spaces $\{|a\rangle\}, \{|b\rangle\}$, where the state labels range from $a, b = 1 \dots 4M$. They are product spaces i.e. $\{|a\rangle\} = \{|l\rangle\} \otimes \{|n_l\rangle\}$ and $\{|b\rangle\} = \{|n_r\rangle\} \otimes \{|r\rangle\}$.

During blocking, the matrix elements of operators on block \mathcal{A} and block \mathcal{B} are formed from the matrix elements of constituent operators on the blocks \mathcal{L}, \bullet_l and \bullet_r, \mathcal{R} respectively. Consider the operations to form the matrix representation of $\hat{A}_{ij} = a_i^\dagger a_j^\dagger$ on block \mathcal{A} . We write this as $\mathbf{A}_{ij}[\mathcal{A}]$, where the bold font denotes matrix representation. Depending on the indices i, j , the matrix representation $(\mathbf{A}_{ij}[\mathcal{A}])_{aa'} = \langle a | a_i^\dagger a_j^\dagger | a' \rangle$ is formed in one of three ways,

$$\begin{aligned}
i, j \in \mathcal{L} &\Rightarrow \mathbf{A}_{ij}[\mathcal{L}] \otimes \mathbf{1}[\bullet_l] \\
i \in \mathcal{L}, j \in \bullet_l &\Rightarrow \mathbf{a}_i[\mathcal{L}] \otimes \mathbf{a}_j[\bullet_l] \\
i, j \in \bullet_l &\Rightarrow \mathbf{1}[\mathcal{L}] \otimes \mathbf{A}_{ij}[\bullet_l]
\end{aligned} \tag{2}$$

Here \otimes denotes a tensor product between operators that is defined with a parity factor to take into account fermion statistics. For two operators \hat{X} and \hat{Y} with matrix elements $\langle \mu | \hat{X} | \mu' \rangle, \langle \nu | \hat{Y} | \nu' \rangle$, the tensor product is defined through

$$\langle \mu\nu | \hat{X}\hat{Y} | \nu'\mu' \rangle = \mathcal{P}(\nu, \hat{X}) \langle \mu | \hat{X} | \mu' \rangle \langle \nu | \hat{Y} | \nu' \rangle \tag{3}$$

where \mathcal{P} is the fermionic parity operator. Similarly, the Hamiltonian matrix $\mathbf{H}[\mathcal{A}]$ is built from the matrix representations of operators in Table II acting on blocks \mathcal{L}, \bullet_l ,

$$\begin{aligned}
\mathbf{H}[\mathcal{A}] &= \mathbf{H}[\mathcal{L}] \otimes \mathbf{1}[\bullet_l] + \mathbf{1}[\mathcal{L}] \otimes \mathbf{H}[\bullet_l] \\
&+ \frac{1}{2} \sum_{i \in \mathcal{L}} \left(\mathbf{a}_i^\dagger[\mathcal{L}] \otimes \mathbf{R}_i[\bullet_l] + \mathbf{R}_i^\dagger[\bullet_l] \otimes \mathbf{a}_i[\mathcal{L}] \right) \\
&+ \frac{1}{2} \sum_{i \in \bullet_l} \left(\mathbf{a}_i^\dagger[\bullet_l] \otimes \mathbf{R}_i[\mathcal{L}] + \mathbf{R}_i^\dagger[\mathcal{L}] \otimes \mathbf{a}_i[\bullet_l] \right) \\
&+ \frac{1}{2} \sum_{ij \in \bullet_l} \left(\mathbf{A}_{ij}[\bullet_l] \otimes \mathbf{P}_{ij}[\mathcal{L}] + \mathbf{A}_{ij}^\dagger[\bullet_l] \otimes \mathbf{P}_{ij}^\dagger[\mathcal{L}] \right) \\
&+ \frac{1}{2} \sum_{ij \in \bullet_l} \mathbf{B}_{ij}[\bullet_l] \otimes \mathbf{Q}_{ij}[\mathcal{L}]
\end{aligned} \tag{4}$$

The representation of other operators in Table II for block \mathcal{A} may be constructed by formulae analogous to Eqs. (2) and (4). These formulae are summarised in Appendix A.

Wavefunction solution — Here we solve for a target eigenstate of \hat{H} for the full problem of k orbitals. In DMRG the corresponding Hilbert space is spanned by the product basis of \mathcal{A} and \mathcal{B} , which we refer to as the superblock space $\{|ab\rangle\}$. The corresponding matrix representation of \hat{H} is the superblock Hamiltonian $\mathbf{H}[\mathcal{AB}]$. The superblock Hamiltonian $\mathbf{H}[\mathcal{AB}]$ is (formally) defined from Eq. (4), where \mathcal{A}, \mathcal{B} replace the block labels \mathcal{L}, \bullet_l . Note that we could also rewrite the Hamiltonian formula in Eq. (4) with the labels \mathcal{A} and \mathcal{B} swapped. For efficiency, we use the above

definition when the number of orbitals in block \mathcal{A} is larger than that in block \mathcal{B} , and swap the labels \mathcal{A} and \mathcal{B} when the reverse is true.

The superblock Hamiltonian matrix is never built in practice, as we only wish to obtain one (or a few) eigenvectors. Instead the target wavefunction is expanded in the superblock basis $\{|ab\rangle\}$

$$|\Psi\rangle = \sum_{ab} \mathbf{C}_{ab} |ab\rangle = \sum_{ln_l n_r r} \mathbf{C}_{ln_l n_r r} |ln_l n_r r\rangle \quad (5)$$

and we obtain the eigenvector \mathbf{C} using the Davidson algorithm. The main operation in the Davidson algorithm is the Hamiltonian wavefunction product $\mathbf{H} \cdot \mathbf{C}$. Since \mathbf{H} is partitioned into a sum of products of operators on blocks \mathcal{A} and \mathcal{B} as Eq. (4), this is carried out for each term in the sum, defining suitable intermediates. For example,

$$(\mathbf{A}_{ij}[\mathcal{A}] \otimes \mathbf{P}_{ij}[\mathcal{B}]) \cdot \mathbf{C} = \mathbf{A}_{ij}[\mathcal{A}] \mathbf{C} \mathbf{P}_{ij}^T[\mathcal{B}] \quad (6)$$

and product is efficiently carried out by grouping the terms $(\mathbf{A}_{ij}[\mathcal{A}] \mathbf{C}) \mathbf{P}_{ij}^T[\mathcal{B}]$ or $\mathbf{A}_{ij}[\mathcal{A}] (\mathbf{C} \mathbf{P}_{ij}^T[\mathcal{B}])$, where superscript T corresponds to the transpose of the operator.

Renormalization and decimation — Here the many-body space of block \mathcal{A} is truncated from dimension $4M$ to dimension M , to obtain the states and operators of the next \mathcal{L} block in the sweep. As argued by White [3], the optimal truncated space is formed by the eigenvectors of the density matrix of \mathcal{A} with the largest eigenvalues. The density matrix is defined by tracing out the contributions of the right block \mathcal{B} to the full density matrix,

$$\hat{\Gamma} = \text{Tr}_B |\Psi\rangle \langle \Psi| \quad (7)$$

$$\mathbf{\Gamma} = \mathbf{C} \mathbf{C}^\dagger \quad (8)$$

The eigenvectors are obtained from

$$\hat{\Gamma} |l\rangle = \sigma_l |l\rangle \quad (9)$$

and the M largest eigenvalues yield a set of eigenstates $\{|l\rangle\}$, $l = 1 \dots M$. We can collect the eigenvectors into a transformation matrix \mathbf{L} , where

$$\mathbf{\Gamma} \mathbf{L} = \mathbf{L} \text{diag}[\sigma_1, \dots, \sigma_M]. \quad (10)$$

The remaining eigenvalues of the discarded eigenstates, $\sigma_{M+1} \dots \sigma_{4M}$ may be summed to give a total discarded weight, which measures the accuracy of the DMRG truncation and which can be used in DMRG extrapolation to the $M = \infty$ limit. To complete the renormalization, we need to convert block \mathcal{A} into a new left block \mathcal{L} . To do this, we truncate the basis $\{|a\rangle\}$ to the renormalised space $\{|l\rangle\}$ of dimension M as above. We next project all the operators constructed on \mathcal{A} into this renormalised space. The projection is written in terms of the density matrix eigenvectors. For an operator $\mathbf{X}[\mathcal{A}]$, we have,

$$\mathbf{X}[\mathcal{L}] = \mathbf{L}^\dagger \mathbf{X}[\mathcal{A}] \mathbf{L} \quad (11)$$

At the end of the decimation step, we have constructed both the space and the operators of the new block \mathcal{L} , and we can proceed to the next sweep iteration.

For efficient calculations, an additional operation is performed after renormalisation and decimation. The convergence of the Davidson algorithm is greatly improved with a good initial guess for the coefficients \mathbf{C} . We can transform the converged coefficients \mathbf{C} obtained during one step of the sweep, to obtain a guess \mathbf{G} for the wavefunction at the next step. This wavefunction transformation uses the forward transformation matrix \mathbf{L} obtained above (for block \mathcal{L}_p), as well as the backward transformation matrix \mathbf{R} (for block \mathcal{R}_{p+1}) obtained from a backwards sweep.

The guess wavefunction is then constructed as

$$\mathbf{G}_{l_p n_{p+1}, n_{p+2} r_{p+3}} = \sum_{\substack{l_{p-1} n_p \\ r_{p+1}}} \tilde{\mathbf{L}}_{l_p, l_{p-1} n_p} \mathbf{R}_{n_{p+2} r_{p+3}, r_{p+2}} \mathbf{C}_{l_{p-1} n_p, n_{p+1} r_{p+2}} \quad (12)$$

where $\tilde{\mathbf{L}}$ is the pseudo-inverse of \mathbf{L} .

A. Abelian symmetries in the DMRG

Abelian symmetries, which include, for example, the axial spin component m , total particle number N , and Abelian point group symmetry, are taken into account in a straightforward manner in the DMRG. We label each block basis state $|\mu\rangle$ by an additional set of quantum numbers q corresponding to the irreducible representations of all the applicable symmetries, i.e.

$$|\mu\rangle \rightarrow |\mu q\rangle \quad (13)$$

For a product state, such as formed in the blocking step, Abelian symmetry means that the quantum numbers of the product state are just the “sum” of quantum numbers of the individual states

$$\begin{aligned} |\mu q\rangle &= |\mu_1 q_1 \mu_2 q_2\rangle \\ q &= q_1 \oplus q_2 \end{aligned} \quad (14)$$

In the case of N and m , \oplus is given by standard addition (i.e. $N = N_1 + N_2$) while in the case of point groups, it is given by modulo addition.

The target eigenstate obtained from DMRG transforms according to a desired irreducible representation. Consequently only many body states $|a\rangle$ and $|b\rangle$ whose quantum numbers sum to the target state quantum numbers need appear in the wavefunction expansion,

$$\begin{aligned} |\Psi_q\rangle &= \sum_{ab} \mathbf{C}_{aq_a bq_b} |aq_a bq_b\rangle \\ q &= q_a \oplus q_b \end{aligned} \quad (15)$$

and thus Abelian symmetry can significantly reduce the number of coefficients in \mathbf{C} .

Operators on the blocks can also be labelled by Abelian symmetry representations or quantum numbers. For example, $a_{i\beta}^\dagger$ is labelled by particle quantum number 1 and m quantum number $-1/2$, reflecting how the operator changes the quantum numbers of the states that it acts on. The labelling of operators by quantum numbers allows the use of selection rules to store and manipulate only the non-zero elements of the operators. These take the form

$$\langle \mu_1 q_1 | \hat{X}^q | \mu_2 q_2 \rangle = \delta_{q_1, q \oplus q_2} \langle \mu_1 q_1 | \hat{X}^q | \mu_2 q_2 \rangle \quad (16)$$

Labelling states and operators using Abelian symmetry thus leads to the following computational advantages: it reduces the number of states that need to be considered on each block, since they need to combine to yield the quantum numbers of the target wavefunction, it limits the coefficients \mathbf{C} in the wavefunction expansion, and, selection rules allow us to work with only non-zero elements of the operators.

III. SPIN ADAPTATION OF THE DMRG ALGORITHM

As discussed in the introduction, the incorporation of spin symmetry can potentially yield significant computational advantages in the DMRG algorithm. The basic advantages are similar to those for Abelian symmetries: elimination of block states which cannot participate in the final target wavefunction, restriction of coefficients in the wavefunction expansion, and selection rules to work with only the non-zero operator elements. However, the non-Abelian nature of the $SU(2)$ Lie group brings additional features into play. For example, associated with every spin state S is a $2S + 1$ degenerate manifold of multiplet states, but if we are interested in the expectation value of a rotationally invariant operator such as the Hamiltonian, then we can work with multiplets as a single entity, rather than working with the individual states. The target wavefunction is then expanded in terms of a set of *reduced coefficients* labelled by multiplets, rather than states. Similarly operators are represented by *reduced matrix elements*, labelled by multiplets rather than states. For a given particle number N in an orbital space of size k , the relative dimension of the number of multiplets of spin S versus the dimension of the state space with axial spin $m = S$ is given by the ratio of the Weyl formula for the number of configuration state functions (with $m = S$) and the formulae for the number of determinants, namely

$$\begin{aligned} \text{no. CSF} &= \frac{2S+1}{k+1} \binom{k+1}{n/2-S} \binom{k+1}{n/2+S+1} \\ \text{no. dets} &= \binom{k}{n/2+m} \binom{k}{n/2-m} \end{aligned} \quad (17)$$

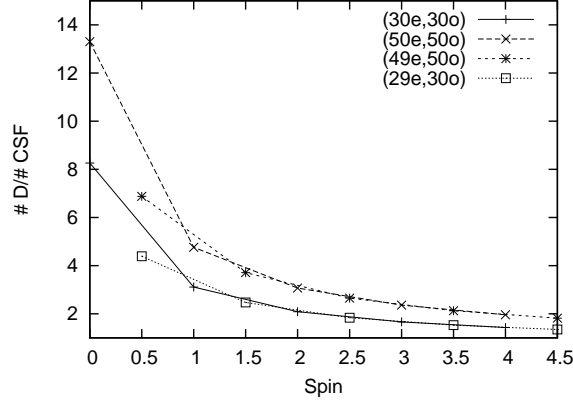


FIG. 2: The figure shows the ratio of the the number of determinants to the number of configuration state functions of a given m and S respectively that can be produced with an active space shown in the legend.

The computational advantage of using the multiplet space, versus the state space, is therefore a function of the particle number, number of orbitals, and spin. Some typical ratios are shown in Fig. 2. We see that the number of multiplets can be much smaller than the number of states, and thus the computational advantages of using the reduced representations can be substantial, particularly when S is small.

Of course, working with the reduced multiplet representations introduces some complications which involve the algebra of $SU(2)$. We now recap the theory of spin eigenstates and spin tensor operators as relevant to the DMRG, before describing the application to the steps of the sweep iteration.

A. Spin eigenstates

Spin symmetry introduce two additional quantum numbers, S and m

$$|\mu\rangle \rightarrow |\mu S m\rangle. \quad (18)$$

Each S is associated with a degenerate multiplet of $2S + 1$ m states, which transform amongst each other under rotation. The non-Abelian character of spin is apparent when we construct spin eigenstates from two underlying spins. In this case $|Sm\rangle$ is not the product of spin eigenstates $|S_1 m_1 S_2 m_2\rangle$, but instead a linear combination of product states with different m_1 and m_2 , coupled by Clebsch-Gordan coefficients $c_{mm_1 m_2}^{SS_1 S_2}$,

$$|Sm\rangle = \sum_{m_1 m_2} c_{mm_1 m_2}^{SS_1 S_2} |S_1 m_1 S_2 m_2\rangle \quad (19)$$

$$m = m_1 + m_2 \quad (20)$$

$$S \in \{|S_1 - S_2|, |S_1 - S_2| + 1, \dots, (S_1 + S_2)\} \quad (20)$$

Eq. (20) generalizes Eq. (14) for Abelian symmetry, to spin symmetry. Because of the restriction in the range of allowed S_1, m_1, S_2, m_2 from Eqs. (19) and (20), we observe that spin confers a similar advantage to an Abelian symmetry in a DMRG calculation: block states on \mathcal{A}, \mathcal{B} need not be considered if they cannot combine to yield the S, m quantum numbers in the target wavefunction.

As mentioned above when solving the Schrödinger equation with spin symmetry we can work with multiplets as a single entity, rather than individual states, because \hat{H} is invariant under rotation. *Reduced quantities* are labelled only by S , and the *reduced* wavefunction is written as

$$|\Psi_S\rangle = \sum_{a S_a b S_b} \mathbf{C}_{a S_a b S_b} |a S_a b S_b\rangle \quad (21)$$

The reduced coefficients in the multiplet representation are related to the coefficients $\mathbf{C}_{a S_a m_a b S_b m_b}$ in the state representation,

$$|\Psi_{Sm}\rangle = \sum_{a S_a m_a b S_b m_b} \mathbf{C}_{a S_a m_a b S_b m_b} |a S_a m_a b S_b m_b\rangle \quad (22)$$

by,

$$\mathbf{C}_{aS_a m_a b S_b m_b} = c_{m_a m_b m}^{S_a S_b S} \mathbf{C}_{aS_a b S_b} \quad (23)$$

The reduced coefficients $\mathbf{C}_{aS_a b S_b}$ are clearly smaller in number than the original set of wavefunction coefficients $\mathbf{C}_{aS_a m_a b S_b m_b}$.

B. Spin tensor operators

With spin, symmetry operators can also acquire labels S, m . Operators which transform according to irreducible spin representations are known as irreducible (spin) tensor operators. Similarly to a spin multiplet, tensor operators labelled by S are associated with a manifold of $2S + 1$ operators that transform amongst each other under rotation. A simple way to characterize a tensor operator is to observe its effect on a state with spin $S = 0$. For example, $a_{i\alpha}^\dagger$ and $a_{i\beta}^\dagger$ are 2 components of a $S = \frac{1}{2}$ (doublet) tensor operator $a^{1/2}$, because they act on a vacuum state (with spin $S = 0$) to generate eigenstates of spin $\frac{1}{2}$. Considering the operators $a_{i\alpha}^\dagger a_{j\alpha}, a_{i\alpha}^\dagger a_{j\beta}, a_{i\beta}^\dagger a_{j\alpha}, a_{i\beta}^\dagger a_{j\beta}$, they collectively span an $S = 0$ singlet and an $S = 1$ triplet manifold. The $S = 0$ singlet operator is defined as

$$\hat{B}_{ij}^{0,0} = \frac{1}{\sqrt{2}}(a_{i\alpha}^\dagger a_{j\alpha} + a_{i\beta}^\dagger a_{j\beta}) \quad (24)$$

and the $S = 1$ triplet operators are defined as

$$\hat{B}_{ij}^{1,-1} = a_{i\beta}^\dagger a_{j\alpha} \quad (25)$$

$$\hat{B}_{ij}^{1,0} = \frac{1}{\sqrt{2}}(a_{i\alpha}^\dagger a_{j\alpha} - a_{i\beta}^\dagger a_{j\beta}) \quad (26)$$

$$\hat{B}_{ij}^{1,1} = -a_{i\alpha}^\dagger a_{j\beta} \quad (27)$$

A full list of the tensor operators used in the spin-adapted DMRG algorithm is given in Table II.

Tensor operators allow us to work with reduced operator matrix elements, labelled only by multiplets

$$\mathbf{X}_{\mu_1 S_1 \mu_2 S_2}^S = \langle \mu_1 S_1 || \hat{X}^S || \mu_2 S_2 \rangle \quad (28)$$

The full matrix elements are obtained from the reduced matrix elements by the Wigner-Eckart theorem (analogously to Eq. (23))

$$\mathbf{X}_{\mu_1 S_1 m_1 \mu_2 S_2 m_2}^{Sm} = c_{m_2 m m_1}^{S_2 S S_1} \mathbf{X}_{\mu_1 S_1 \mu_2 S_2}^S \quad (29)$$

The adjoint of a tensor operator is also a tensor operator. Here, we define the adjoint with a additional sign factor to preserve the Condon-Shortley phase convention used in the angular momentum ladder operators. To denote this adjoint with an additional phase, we use the symbol \ddagger . For example

$$\mathbf{X}^{S,m\dagger} = (-1)^{S+m} \mathbf{X}^{S,-m\dagger} \quad (30)$$

Note that reduced matrix elements of the adjoint of a tensor operator are not the adjoint of the reduced matrix elements of the operator. The relationship between the reduced matrix elements of the tensor operators of spin $S = 0, \frac{1}{2}, 1$ and those of the corresponding adjoint operators, is given in Appendix C 1.

As is the case for spin eigenstates, a product tensor operator with quantum numbers S, m consists of a linear combination of tensor operators with quantum numbers S_1, m_1 and S_2, m_2 , coupled through Clebsch-Gordan coefficients

$$(\hat{X}_1^{S_1} \hat{X}_2^{S_2})^{Sm} = \sum_{m_1 m_2} c_{m_1 m_2 m}^{S_1 S_2 S} \hat{X}_1^{S_1 m_1} \hat{X}_2^{S_2 m_2} \quad (31)$$

We can obtain the reduced matrix elements of the product operator $(\hat{X}_1^{S_1} \hat{X}_2^{S_2})^S$ directly from the reduced matrix elements of the operators \hat{X} and \hat{Y} using Wigner 9j coefficients

$$\begin{aligned} & \langle \mu\nu S_{\mu\nu} || (\hat{X}_1^{S_1} \hat{X}_2^{S_2})^S || \mu'\nu' S_{\mu'\nu'} \rangle \\ &= \begin{bmatrix} S_{\mu'} & S_{\nu'} & S_{\mu\nu'} \\ S_1 & S_2 & S \\ S_\mu & S_\nu & S_{\mu\nu} \end{bmatrix} \langle \mu S_\mu || X_1^{S_1} || \mu' S_{\mu'} \rangle \langle \nu S_\nu || X_2^{S_2} || \nu' S_{\nu'} \rangle \end{aligned} \quad (32)$$

Here we define the spin-adapted tensor product \otimes_S as

$$\left(\mathbf{X}_1^{S_1} \mathbf{X}_2^{S_2}\right)^S = \mathbf{X}_1^{S_1} \otimes_S \mathbf{X}_2^{S_2} \quad (33)$$

which is the reduced matrix analogue of Eq. (31) and the reduced matrix elements of $\left(\mathbf{X}_1^{S_1} \mathbf{X}_2^{S_2}\right)^S$ are calculated as shown in Eq. (32).

We now proceed to discuss how the spin algebra established above can be applied to the computations of the sweep iteration.

C. Spin-adapted sweep iteration

Blocking — The two modifications to blocking when implementing spin-adaptation, are (i) instead of using the operators in Table II, we use tensor operators, defined in Table II, (ii) because we use tensor operators, we manipulate and store only the reduced matrix elements of the operators. This means that we replace the tensor multiplication \otimes , by the spin-adapted tensor multiplication \otimes_S , defined in Eq. (33).

As an example, we consider the $A_{ij}^S[\mathcal{A}]$ spin tensor operators, whose non-tensor analogues were considered in Eq. (2). The matrix of reduced matrix elements corresponding to $A_{ij}^0[\mathcal{A}]$ is obtained by

$$\begin{aligned} i, j \in \mathcal{L} &\Rightarrow \mathbf{A}_{ij}^0[\mathcal{L}] \otimes_0 \mathbf{1}^0[\bullet_l] \\ i \in \mathcal{L}, j \in \bullet_l &\Rightarrow \mathbf{a}_i^{1/2}[\mathcal{L}] \otimes_0 \mathbf{a}_j^{1/2}[\bullet_l] \\ i, j \in \bullet_l &\Rightarrow \mathbf{1}^0[\mathcal{L}] \otimes_0 \mathbf{A}_{ij}^0[\bullet_l] \end{aligned} \quad (34)$$

The partitioning of the superblock Hamiltonian similarly follows Eq. (4). Here we recall that the Hamiltonian is an $S = 0$ operator, i.e. we write \mathbf{H}^0 . Then

$$\begin{aligned} \mathbf{H}^0[\mathcal{A}] &= \mathbf{H}^0[\mathcal{L}] \otimes_0 \mathbf{1}^0[\bullet_l] + \mathbf{1}^0[\mathcal{L}] \otimes_0 \mathbf{H}^0[\bullet_l] \\ &+ 2 \sum_{i \in \mathcal{L}} \left(\mathbf{a}_i^{1/2}[\mathcal{L}] \otimes_0 \mathbf{R}_i^{1/2\dagger}[\bullet_l] + \mathbf{a}_i^{1/2\dagger}[\mathcal{L}] \otimes_0 \mathbf{R}_i^{1/2}[\bullet_l] \right) \\ &+ 2 \sum_{i \in \bullet_l} \left(\mathbf{a}_i^{1/2}[\bullet_l] \otimes_0 \mathbf{R}_i^{1/2\dagger}[\mathcal{L}] + \mathbf{a}_i^{1/2\dagger}[\bullet_l] \otimes_0 \mathbf{R}_i^{1/2}[\mathcal{L}] \right) \\ &+ \sum_{ij \in \bullet_l} \left(-\sqrt{3} \mathbf{B}_{ij}^1[\bullet_l] \otimes_0 \mathbf{Q}_{ij}^1[\mathcal{L}] + \mathbf{B}_{ij}^0[\bullet_l] \otimes_0 \mathbf{Q}_{ij}^0[\mathcal{L}] \right) \\ &+ \frac{\sqrt{3}}{2} \sum_{ij \in \bullet_l} \left(\mathbf{A}_{ij}^1[\bullet_l] \otimes_0 \mathbf{P}_{ij}^1[\mathcal{L}] + \mathbf{A}_{ij}^{1\dagger}[\bullet_l] \otimes_0 \mathbf{P}_{ij}^{1\dagger}[\mathcal{L}] \right) \\ &+ \frac{1}{2} \sum_{ij \in \bullet_l} \left(\mathbf{A}_{ij}^0[\bullet_l] \otimes_0 \mathbf{P}_{ij}^0[\mathcal{L}] + \mathbf{A}_{ij}^{0\dagger}[\bullet_l] \otimes_0 \mathbf{P}_{ij}^{0\dagger}[\mathcal{L}] \right) \end{aligned} \quad (35)$$

Wavefunction solution — In the wavefunction solution step, the spin-adapted Hamiltonian wavefunction product can be performed entirely in terms of the reduced operator matrix elements and reduced wavefunction coefficients. As in non-spin adapted DMRG algorithm, the full Hamiltonian matrix is never generated and the product is carried out for each term in the sum in the Hamiltonian in Eq. (35). For example, Eq. (6) becomes

$$\begin{aligned} \mathbf{C}_{a'S'_a b'S'_b} &= \\ \sum_{S_a S_b} \begin{bmatrix} S_b & S_a & S \\ S_J & S_I & 0 \\ S'_b & S'_a & S' \end{bmatrix} &\langle S'_b || \mathbf{O}_J^{S_J}[\mathcal{B}] || S_b \rangle \langle S'_a || \mathbf{O}_I^{S_I}[\mathcal{A}] || S_a \rangle \mathbf{C}_{a S_a b S_b} \end{aligned} \quad (36)$$

Note, however, because of the appearance of the $9j$ coefficients, the operator product does not separate into two decoupled multiplets, as in the non-spin adapted case shown in Eq. (6). This leads to some overhead in the spin-adapted algorithm relative to the non-spin-adapted case, depending on the number of $9j$ coefficients that need to be considered.

TABLE II: Definition of the operators used in the spin-adapted DMRG. Here the indices are spatial indices not spin indices.

Label	Operator	Tensor Operator Label
$a_i^{1/2,-1/2}$	$a_{i\beta}^\dagger$	$a_i^{1/2}$
$a_i^{1/2,1/2}$	$a_{i\alpha}^\dagger$	
$R_k^{1/2,-1/2}$	$\frac{1}{\sqrt{2}} \sum_{ijl} \nu_{ijkl} (a_{i\alpha}^\dagger a_{j\alpha}^\dagger a_{l\alpha} + a_{i\alpha}^\dagger a_{j\beta}^\dagger a_{k\beta})$	$R_k^{1/2}$
$R_k^{1/2,1/2}$	$\frac{1}{\sqrt{2}} \sum_{ijl} \nu_{ijkl} (a_{i\beta}^\dagger a_{j\alpha}^\dagger a_{k\alpha} + a_{i\beta}^\dagger a_{j\beta}^\dagger a_{k\beta})$	
$A_{ij}^{0,0}$	$\frac{1}{\sqrt{2}} (a_{i\alpha}^\dagger a_{j\beta}^\dagger - a_{i\beta}^\dagger a_{j\alpha}^\dagger)$	A_{ij}^0
$A_{ij}^{1,-1}$	$a_{i\beta}^\dagger a_{j\beta}^\dagger$	A_{ij}^1
$A_{ij}^{1,0}$	$\frac{1}{\sqrt{2}} (a_{i\alpha}^\dagger a_{j\beta}^\dagger + a_{i\beta}^\dagger a_{j\alpha}^\dagger)$	
$A_{ij}^{1,1}$	$a_{i\alpha}^\dagger a_{j\alpha}^\dagger$	
$B_{ij}^{0,0}$	$\frac{1}{\sqrt{2}} (a_{i\alpha}^\dagger a_{j\alpha} + a_{i\beta}^\dagger a_{j\beta})$	B_{ij}^0
$B_{ij}^{1,-1}$	$a_{i\beta}^\dagger a_{j\alpha}$	B_{ij}^1
$B_{ij}^{1,0}$	$\frac{1}{\sqrt{2}} (a_{i\alpha}^\dagger a_{j\alpha} - a_{i\beta}^\dagger a_{j\beta})$	
$B_{ij}^{1,1}$	$-a_{i\alpha}^\dagger a_{j\beta}$	
$P_{ij}^{0,0}$	$\frac{1}{\sqrt{2}} \sum_{kl} -\nu_{ijkl} (-a_{l\alpha} a_{k\beta} + a_{l\beta} a_{k\alpha})$	P_{ij}^0
$P_{ij}^{1,-1}$	$\sum_{kl} \nu_{ijkl} a_{l\alpha} a_{k\alpha}$	P_{ij}^1
$P_{ij}^{1,0}$	$\frac{1}{\sqrt{2}} \sum_{kl} -\nu_{ijkl} (-a_{l\alpha} a_{k\beta} - a_{l\beta} a_{k\alpha})$	
$P_{ij}^{1,1}$	$\sum_{kl} \nu_{ijkl} a_{l\beta} a_{k\beta}$	
$Q_{ij}^{0,0}$	$\frac{1}{\sqrt{2}} \sum_{kl} (-\nu_{iklj} + 2\nu_{ikjl}) (a_{k\alpha}^\dagger a_{l\alpha} + a_{k\beta}^\dagger a_{l\beta})$	Q_{ij}^0
$Q_{ij}^{1,-1}$	$\sum_{kl} -\nu_{iklj} a_{k\beta}^\dagger a_{l\alpha}$	Q_{ij}^1
$Q_{ij}^{1,0}$	$\frac{1}{\sqrt{2}} \sum_{kl} -\nu_{iklj} (a_{k\alpha}^\dagger a_{l\alpha} - a_{k\beta}^\dagger a_{l\beta})$	
$Q_{ij}^{1,1}$	$\sum_{kl} \nu_{iklj} a_{k\alpha}^\dagger a_{l\beta}$	

Renormalisation and decimation — In the spin-adapted renormalisation and decimation step we do not seek a simple optimal truncation of the states of \mathcal{A} , but rather an optimal truncation to a set of states consistent with spin symmetry, i.e. to a set of pure spin states. These cannot be obtained as eigenvectors of the reduced density matrix of \mathcal{A} , because it does not commute with the spin operator \hat{S}^2 of block \mathcal{A} . As shown in McCulloch *et al.* [29], the density matrix to use in this case is the quasi-density matrix, which is obtained from the usual density matrix by setting off-diagonal blocks, that couple states of different spins, to zero. All operations of the renormalisation and decimation step can be carried out in the multiplet representation, working in terms of reduced wavefunction coefficients and reduced matrix elements. The reduced matrix elements of the quasi-density matrix are obtained from the reduced wavefunction coefficients.

$$\Gamma_{aS_a, a'S_a} = \sum_{bS_b} \mathbf{C}_{aS_a bS_b} \mathbf{C}_{a'S_a bS_b}^* \quad (37)$$

The eigenvectors of the quasi-density matrix yield the transformation matrices in reduced form, via its eigenvectors

$$\hat{\Gamma} ||l_S\rangle = \sigma_{l,S} ||l_S\rangle \quad (38)$$

After obtaining the new renormalized basis, the operators in multiplet representation are transformed using the analogous formula to Eq. (11).

Note that when retaining M eigenvectors of the quasi-density matrix in the multiplet representation, we are retaining M sets of spin-multiplets. This corresponds to a much larger set of underlying states, which is of course, the advantage of working in a spin-adapted formulation. However we will still use the terminology “ M states” to refer to the renormalized basis in the spin-adapted algorithm.

As described in the non-spin adapted case, the convergence of the Davidson iteration is greatly improved if we use a suitable guess obtained by transforming the wavefunction from the previous sweep iteration. The transformation of the wavefunction in the case of the spin-adapted algorithm is very similar to the case of the non-spin-adapted algorithm with the exception that a spin-rescaling step must be performed, involving the Racah coefficients. Eq. (39) is analogous to Eq. (12), but in the last step we explicitly specify the spin quantum number of each multiplet state because these are required in the Racah coefficients W . In Eq. (40) instead of matrix coefficients we use the bra-ket notation, to explicitly show the couplings of the spins, so for example $\mathbf{G}_{l_p, n_{p+1} n_{p+2} r_{p+3}}$ is the same as $\langle l_{p;S_1} | \langle n_{p+1;S_2} (n_{p+2;S_3} r_{p+3;S_4} (S_5)) (S_{25}) | \Psi(S) \rangle$, where states $n_{p+2;S_3}$ and $r_{p+3;S_4}$ couple to form a state with spin S_5 , which in turn couples to state $n_{p+1;S_2}$ to form a state with spin S_{25} .

$$\mathbf{G}_{l_p, n_{p+1} n_{p+2} r_{p+3}} = \sum_{\substack{l_{p-1} n_p \\ r_{p+1}}} \tilde{\mathbf{L}}_{l_p, l_{p-1} n_p} \mathbf{R}_{n_{p+2} r_{p+3}, r_{p+2}} \mathbf{C}_{l_{p-1} n_p, n_{p+1} r_{p+2}} \quad (39)$$

$$\begin{aligned} \langle l_{p;S_1} n_{p+1;S_2} (S_{12}) | \langle n_{p+2;S_3} r_{p+3;S_4} (S_5) | \Psi(S) \rangle = \\ \sum_{\substack{l_p n_{p+1} \\ r_{p+2}}} W(S_1 S_2 S S_5; S_{12} S_{25}) [(2S_{12} + 1)(2S_{23} + 1)]^{1/2} \times \\ \langle l_{p;S_1} | \langle n_{p+1;S_2} (n_{p+2;S_3} r_{p+3;S_4} (S_5)) (S_{25}) | \Psi(S) \rangle \end{aligned} \quad (40)$$

IV. COMPUTATIONAL CONSIDERATIONS

The computational implementation of the spin-adapted DMRG algorithm is similar to the non-spin-adapted DMRG. Here we focus on computational differences between the two.

- The total number of operators stored in the spin-adapted DMRG is approximately half that in the non-spin-adapted DMRG. The most numerous kinds of operators in the DMRG algorithm are those with two orbital indices i and j , namely $\hat{A}_{ij}, \hat{B}_{ij}, \hat{P}_{ij}, \hat{Q}_{ij}$. In the non-spin-adapted case there are four different \hat{A}_{ij} operators for every spatial pair ij , i.e. $\hat{A}_{i\alpha j\alpha}, \hat{A}_{i\beta j\alpha}, \hat{A}_{i\alpha j\beta},$ and $\hat{A}_{i\beta j\beta}$. In the spin-adapted case, there are only two tensor operators: \hat{A}_{ij}^0 and \hat{A}_{ij}^1 . \hat{A}_{ij}^1 contains three m components, but the Wigner-Eckart theorem (Eq. (29)) means we store only a *single* matrix of reduced matrix elements.
- The storage dependence of the spin-adapted algorithm is $O(M^2)$ which is the same scaling as in the non-spin-adapted algorithm. However, the storage prefactor in the spin-adapted case is larger. This arises from the non-Abelian nature of the spin symmetry. For example, if we consider an operator such as \hat{B}_{ij}^1 , the following reduced matrix elements are non-zero: $\langle \mu_1 S | \hat{B}_{ij}^1 | \mu_2 S - 1 \rangle$, $\langle \mu_1 S | \hat{B}_{ij}^1 | \mu_2 S \rangle$ and $\langle \mu_1 S | \hat{B}_{ij}^1 | \mu_2 S + 1 \rangle$ i.e. several different couplings between bra and ket are allowed. When Abelian symmetries are used, $\hat{B}_{i\alpha j\beta}$ has non-zero matrix elements only between states of a single type $\langle \mu_1 m |$ and $| \mu_2 m \rangle$.
- The main cost of the algorithm comes from the Hamiltonian wavefunction multiplication in the wavefunction solution step, and the operator transformation, in the renormalisation and decimation step. In the spin-adapted case, the cost of the Hamiltonian wavefunction multiplication is $O(k^2 M^3)$ per sweep step, similar to the non-spin-adapted algorithm. In the spin-adapted algorithm the presence of the $9j$ coupling coefficients prevents the Hamiltonian wavefunction multiplication from factoring into two stages as in Eq. (6). The prefactor of this step thus depends on the number of $9j$ couplings that must be accounted for. For singlet states, the spin-adapted computational prefactor is similar to that of the non-spin-adapted case but for higher spin states, it can be larger. The operator transformation in the spin-adapted algorithm is very similar to the non-spin-adapted case (and scales as $O(k^2 M^3)$ per sweep step) except for the fact that some of the operators are more dense as described in the previous paragraph.
- For large scale calculations an efficient parallelization of the code is required. We have carried this out in the exact same way as in the non-spin-adapted DMRG algorithm described by Chan[36].

A. Singlet Embedding

When using the spin-adapted DMRG algorithm to study higher spin states than the singlet, some disadvantages appear. Firstly, the reduced coefficient matrix $\mathbf{C}_{aS_a bS_b}$ becomes more dense. In the case of the singlet, only quantum states of equal spins on blocks \mathcal{A} and \mathcal{B} can couple, while for say, a triplet state, additional couplings ($S_b = S_a \pm 1$) are possible. A second disadvantage (related to the first) is that for non-singlet states, the eigenvalues of the quasi-density matrix of block \mathcal{A} and of block \mathcal{B} are not equivalent. A simple example illustrates this. Consider a reduced wavefunction written as

$$||\Psi_{S=1}\rangle = \frac{1}{\sqrt{2}}||aS_a = 1\rangle(||bS_b = 0\rangle + ||bS_b = 2\rangle) \quad (41)$$

The quasi-density matrix of block \mathcal{A} has one non-zero eigenvalue, while that of block \mathcal{B} has two non-zero eigenvalues. This non-equivalence means that discarded weights obtained during the forward and backward sweeps of a calculation (which respectively arise from quasi-density matrices of blocks \mathcal{A} and \mathcal{B}) are different, and this makes DMRG energy extrapolation using discarded weights ambiguous.

To overcome these disadvantages, it is clearly best to use the spin-adapted algorithm only to target singlet states. How then do we study systems in a higher spin state? One way is to use a technique which we call singlet embedding, originally introduced by Nishino *et al.*[2]. Here we note that we can always add a set of auxiliary non-interacting orbitals to the end of the lattice which couple to the physical orbitals to overall yield a singlet state. In general, the wavefunction $||\tilde{\Psi}\rangle$ of the combined physical and auxiliary orbitals is of the form

$$||\tilde{\Psi}_{S=0}\rangle = ||\Psi_S\rangle||\Phi_S\rangle \quad (42)$$

where $||\Phi_S\rangle$ is the state of the auxiliary non-interacting orbitals. Because the auxiliary orbitals do not energetically couple to the physical system, and have themselves no energy, they do not affect the energy of the physical system. We have implemented the singlet embedding technique as an option in our calculations, as described below.

V. APPLICATIONS

In this section we describe application of spin-adapted DMRG algorithm to study two small transition metal complexes, Fe_2S_2 [37, 38] and Cr_2 [39–41] which have been of interest in quantum chemistry. In the first calculation, we target the spin ladder of the Fe_2S_2 molecule. Here we use a small active space of 12 electrons in 12 orbitals ($12e, 12o$) and a minimal basis[42], to demonstrate the ability of the spin-adapted DMRG algorithm to target very closely spaced states of different spatial and spin symmetries. In our second calculation, we study the singlet and triplet spin states of the Cr_2 molecule. This is a benchmark calculation using a large active space ($24e, 30o$) but a small (single-valence) basis set, that follows closely the earlier work of Kurashige and Yanai on the same system. This calculation is primarily intended to examine the relative efficiencies of the spin-adapted and non-spin-adapted algorithms.

A. Fe_2S_2

We first carried out spin-adapted DMRG calculations on the Fe_2S_2 molecule. The geometry, which exhibits D_{2h} point group symmetry, is given in Table III. We used a minimal STO-3G[42] basis. The active space was identified by carrying out a high-spin UB3LYP/STO-3G[42–44] calculation with multiplicity 9 (eight unpaired electrons), and then selecting 12 unrestricted natural orbitals with occupation numbers between 1.99 and 0.01 to make up the ($12e, 12o$) active space. The order of the orbitals in the DMRG calculation was by occupation number. We then carried out calculations on 40 states (multiplicities 1, 3, 5, 7, 9, for each of the 8 irreps of D_{2h}). With $M=200$ the DMRG energies (in E_h) were already converged to 5 decimal places as compared to the ORCA[45] complete active space configuration interaction (CASSI) results.

The corresponding energies are given in Table IV. As can be seen, many of the states are nearly degenerate (to within $<10\mu\text{H}$) and thus would be extremely hard to resolve without a spin-adapted algorithm.

TABLE III: Cartesian coordinates of Fe_2S_2 with D_{2h} symmetry. The molecule lies in the yz plane.

Atom	y	z
	\AA	
S	0.00	-4.29
S	0.00	4.29
Fe	-2.10	0.00
Fe	2.10	0.00

TABLE IV: Energies ($E + 3283.0$) in E_h of Fe_2S_2 in various spin and symmetry states calculated using the spin-adapted DMRG algorithm. The results agree with ORCA CASCI energies to all the decimal places shown. Note the very close spacing of the states, which would be very hard to resolve without a spin-adapted algorithm.

Irrep	Multiplicity				
	1	3	5	7	9
A_g	-0.75990	-0.75990	-0.75993	-0.75993	-0.75996
B_{1g}	-0.75992	-0.75992	-0.75991	-0.75993	-0.75996
B_{2g}	-0.77343	-0.78351	-0.78343	-0.72207	-0.78312
B_{3g}	-0.77345	-0.78007	-0.77991	-0.78662	-0.78648
A_u	-0.76308	-0.77344	-0.78678	-0.78669	-0.78656
A_{1u}	-0.77686	-0.77672	-0.78333	-0.72207	-0.78301
A_{2u}	-0.68761	-0.75991	-0.75990	-0.75992	-0.75995
A_{3u}	-0.69535	-0.75991	-0.75993	-0.69537	-0.69614

B. Cr_2

Recently Kurashige and Yanai[11] carried out large-scale DMRG calculations on the singlet ground state of Cr_2 using an active space of $(24e, 30o)$. These were benchmark rather than realistic calculations because they used a small single valence (SV) basis set which did not include dynamical correlation (see however Ref. [46] for a more detailed DMRG with perturbation theory study of the chromium dimer with the inclusion of dynamical correlation). Here, we use the same Cr_2 benchmark example as Kurashige and Yanai with exactly the same geometry (bond length 1.5 \AA), molecular orbitals and ordering as in their original paper. Our purpose will be to examine the accuracy and speed of the spin-adapted DMRG algorithm as compared to the non-spin-adapted algorithm. We target the singlet (1A_g in D_{2h} symmetry) and triplet ($^3B_{1g}$ in D_{2h} symmetry) states of the molecule in our calculations.

1. Accuracy

TABLE V: Energy in E_h and discarded weights of a spin-adapted DMRG calculation on the singlet state of the Cr_2 molecule. Note that our M=5000 spin-adapted energy is already better than the M=10000 non-spin-adapted energy reported by Kurashige and Yanai [11].

M	Energy(E_h)	Discarded weight
1000	-2086.41831	2.032×10^{-5}
2000	-2086.41979	1.006×10^{-5}
5000	-2086.42061	3.075×10^{-6}
8000	-2086.42078	1.608×10^{-6}
10000	-2086.42082	9.630×10^{-7}
∞	-2086.42100	

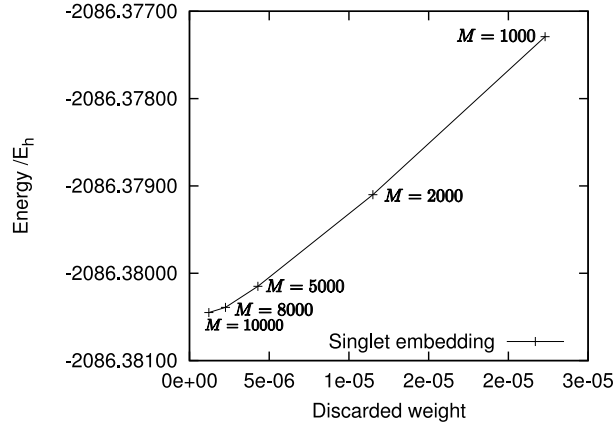


FIG. 3: DMRG energy in E_h of the Cr_2 triplet state on the y-axis versus discarded weight on the x-axis using the singlet embedding approach.

The total DMRG energy of the singlet state as a function of the number of retained states (M), as well as the discarded weight in the quasi-density matrix (the largest discarded weight during the DMRG sweep), is shown in Table V. Kurashige and Yanai’s converged DMRG energy with 10000 non-spin-adapted states was $-2086.42053 E_h$ which is slightly *above* our spin-adapted $M=5000$ energy of $-2086.42061 E_h$. We see that the spin-adapted DMRG algorithm requires roughly only half the number of states as the non-spin-adapted DMRG, to achieve a similar accuracy in the energy. The greater accuracy of the spin-adapted algorithm allows us to perform a more accurate extrapolation of the DMRG energy to $M = \infty$ than in [11] and our final $M = 10000$ spin-adapted DMRG energy is within $0.2 mE_h$ of the extrapolated $M = \infty$ result.

The total DMRG energy and the discarded weights of the triplet state using the spin-adapted (with and without spin embedding) and non-spin-adapted algorithms are shown in Table VI. Similarly to the singlet case, we find that the spin-adapted algorithm requires roughly half the number of renormalised states as the non-spin-adapted algorithm to achieve the same accuracy. Singlet embedding (section IV A), although formally increasing the number of orbitals in the problem, leads to no loss of accuracy as compared to the spin-adapted calculation on the triplet state, and indeed leads to a slight increase in accuracy. As observed in section IV A, in the spin-adapted calculation on the triplet state, the discarded weights obtained during the forward and backward sweeps are vastly different. This discrepancy vanishes when the triplet state energies are obtained via embedding in a singlet state. The singlet embedding allows us to perform energy extrapolation with respect to the discarded weights, as shown in Fig. 3. We find that the $M = 10000$ spin-adapted calculation is within $0.3 mE_h$ of the extrapolated exact DMRG result.

TABLE VI: Energies in E_h and discarded weights of a spin-adapted DMRG calculation on the triplet state of the Cr_2 molecule. Columns 2 through 5 give data for the forward and backward sweeps of spin-adapted calculations, columns 6 and 7 give our results when we use the singlet embedding technique and finally the last two columns give our results of non-spin-adapted calculations.

M	Spin-adapted DMRG						Non-spin-adapted	
	Forward sweep		Backward sweep		Singlet embedding		Energy(E_h)	Discarded weight
	Energy(E_h)	Discarded weight	Energy(E_h)	Discarded weight	Energy(E_h)	Discarded weight		
1000	-2086.37682	1.45×10^{-4}	-2086.37682	1.77×10^{-5}	-2086.37729	2.23×10^{-5}	-2086.37418	5.89×10^{-5}
2000	-2086.37888	6.67×10^{-5}	-2086.37888	1.10×10^{-5}	-2086.37910	1.15×10^{-5}	-2086.37736	2.75×10^{-5}
5000	-2086.38011	2.46×10^{-5}	-2086.38009	4.69×10^{-6}	-2086.38015	4.29×10^{-6}	-2086.37949	1.10×10^{-5}
8000	-2086.38036	1.16×10^{-5}	-2086.38036	2.78×10^{-6}	-2086.38039	2.26×10^{-6}	-2086.38000	5.86×10^{-6}
10000	-2086.38043	8.56×10^{-6}	-2086.38043	1.94×10^{-6}	-2086.38045	1.21×10^{-6}	-2086.38016	3.52×10^{-6}
∞					-2086.38074		-2086.38059	

TABLE VII: Wall clock times for a single Davidson iteration performed with spin-adapted and non-spin-adapted DMRG algorithms on 2 Intel Xeon E5420 processors with 4 cores each. Spin_{se} is the singlet embedding technique where we add a set of non-interacting orbitals and then target the $S = 0$ state of the combined system (see text for more details). Ratio denotes the ratio of the best spin-adapted to non-spin-adapted timings. Note that the singlet embedding technique greatly reduces the cost of the spin-adapted DMRG calculation for the triplet state.

M	S=0			S=1			
	Timings /s			Timings /s			
	Spin	non-Spin	Ratio	Spin	Spin _{se}	non-Spin	Ratio
2000	59	55	1.07	111	41	48	0.85
5000	329	292	1.13	707	248	267	0.93
8000	1003	794	1.26	2622	792	746	1.06
10000	1752	1363	1.29	4628	1782	1295	1.38

2. Efficiency

As explained in Section IV the most expensive step in the DMRG algorithm is formation of the Hamiltonian wavefunction product, whose computational cost scales as $O(M^3)$, where M is the number of retained states. From the above results, we observe that the spin-adapted algorithm requires roughly half the number of renormalised states as the non-spin-adapted algorithm to achieve the same accuracy. This suggests that if the cost of a single Davidson iteration (for a given number of states) is comparable between the spin-adapted and non-spin-adapted algorithms, then, to achieve a given accuracy in the DMRG energy, the spin-adapted algorithm should offer an 8-fold gain in computational speed.

To compare the performance of the spin-adapted and non-spin-adapted DMRG algorithms we show the wall times per Davidson iteration of the two algorithms in Table VII. For the singlet case, we notice that for example the $M = 5000$ timings are comparable for both the spin-adapted and non-spin-adapted calculations. However, moving to $M = 10000$, the computational cost increases by a factor of 4 rather than 8 i.e. more like $O(M^2)$ rather than $O(M^3)$. This means that the spin-adapted algorithm yields (for a given accuracy) only a 4-fold gain in computational efficiency over the non-spin-adapted algorithm. The quadratic scaling is a result of the high Abelian spatial symmetry (D_{2h}) present in the molecule, which means that each of the non-zero blocks of the operators are so small that the corresponding BLAS matrix multiplication operations are dominated by quadratic as opposed to cubic complexity terms. We expect, however, the computational scaling would approach $O(M^3)$ as M is increased further, or if the calculations were performed without the use of point group symmetry, as may be the case in other more complex molecules, in which case the spin-adapted algorithm should offer even larger computational gains.

In the triplet state, as expected from the analysis in section IV, for any given M , the cost of the Davidson iteration is much higher for the spin-adapted algorithm than for the non-spin-adapted algorithm. However, with singlet embedding, the spin-adapted computational times are now similar to those of the non-spin-adapted case. Thus, with singlet embedding, the spin-adapted algorithm also provides a 4-fold efficiency gain for the triplet state, which we expect to rise either as M is increased, or if we consider more complex molecules without high Abelian spatial symmetry.

VI. CONCLUSIONS

In this work we implemented a spin-adapted density matrix renormalization group algorithm that extends the work of McCulloch and Gulacsi to quantum chemical Hamiltonians. The spin-adapted algorithm opens up the individual targetting of closely spaced spin states. Furthermore, when used in conjunction with the singlet embedding technique of Nishino, we find that significant computational gains are possible. In the systems studied here, the number of spin-adapted renormalised states required for a given accuracy is roughly only half that of the non-spin-adapted renormalised states. This yields a theoretical computational speedup of a factor of 8, although we observe speedups closer to 4 due to the high point group symmetry of the systems we have studied. The ability to target individual spin states, as well as the improved computational efficiency of the spin-adapted algorithm, will be particularly advantageous when studying larger transition metal complexes such as those which involve multiple metal centres. Such studies are currently in progress in our group.

VII. ACKNOWLEDGEMENTS

This work was supported by an NSF CHE CAREER grant, NSF-CHE-0645380.

Bibliography

- [1] I. P. McCulloch and M. Gulacsi, *Europhys. Lett.* **57**, 852 (2002).
- [2] W. Tatsuaki, *Phys. Rev. E* **61**, 3199 (2000).
- [3] S. R. White, *Phys. Rev. Lett.* **69**, 2863 (1992).
- [4] S. R. White, *Phys. Rev. B* **48**, 10345 (1993).
- [5] S. R. White and R. L. Martin, *J. Chem. Phys.* **110**, 4127 (1999).
- [6] A. O. Mitrushenkov, G. Fano, F. Ortolani, R. Linguerri, and P. Palmieri, *J. Chem. Phys.* **115**, 6815 (2001).
- [7] G. K. L. Chan and M. Head-Gordon, *J. Chem. Phys.* **116**, 4462 (2002).
- [8] K. H. Marti, I. M. Ondik, G. Moritz, and M. Reiher, *J. Chem. Phys.* **128**, 014104 (2008).
- [9] Ö. Legeza, J. Röder, and B. A. Hess, *Phys. Rev. B* **67**, 125114 (2003).
- [10] D. Zgid and M. Nooijen, *J. Chem. Phys.* **128**, 014107 (2008).
- [11] Y. Kurashige and T. Yanai, *J. Chem. Phys.* **130**, 234114 (2009).
- [12] S. Daul, I. Ciofini, C. Daul, and S. R. White, *Int. J. Quantum Chem.* **79**, 331 (2000).
- [13] A. O. Mitrushenkov, R. Linguerri, P. Palmieri, and G. Fano, *J. Chem. Phys.* **119**, 4148 (2003).
- [14] Ö. Legeza, J. Röder, and B. A. Hess, *Mol. Phys.* **101**, 2019 (2003).
- [15] J. Rissler, R. M. Noack, and S. R. White, *Chem. Phys.* **323**, 519 (2006).
- [16] Ö. Legeza and J. Sólyom, *Phys. Rev. B* **68**, 195116 (2003).
- [17] G. Moritz, B. A. Hess, and M. Reiher, *J. Chem. Phys.* **122**, 024107 (2005).
- [18] G. Moritz and M. Reiher, *J. Chem. Phys.* **124**, 034103 (2006).
- [19] G. Moritz, A. Wolf, and M. Reiher, *J. Chem. Phys.* **123**, 184105 (2005).
- [20] G. Moritz and M. Reiher, *J. Chem. Phys.* **126**, 244109 (2007).
- [21] T. Yanai, Y. Kurashige, E. Neuscamman, and G. K.-L. Chan, *J. Phys. Chem.* **132**, 24105 (2010).
- [22] W. Duch and J. Karwowski, *Int. J. Quantum Chem.* **22**, 783 (1982).
- [23] K. Ruedenberg, *Phys. Rev. Lett.* **27**, 1105 (1971).
- [24] J. Paldus and P. E. S. Wormer, *Int. J. Quantum Chem.* **16**, 1321 (1979).
- [25] I. Shavitt, *Int. J. Quantum Chem.* **14**, 5 (1978).
- [26] B. R. Brooks and H. F. I. Schaefer, *J. Chem. Phys.* **70**, 5092 (1979).
- [27] G. Sierra and T. Nishino, *Nuc. Phys. B* **495**, 505 (1997).
- [28] T. Wada, *Phys. Rev. E* **61**, 3199 (2000).
- [29] I. P. McCulloch and M. Gulacsi, *Aust. J. Phys.* **53**, 597 (2000).
- [30] I. P. McCulloch and M. Gulacsi, *Philos. Mag. Lett.* **81**, 447 (2001).
- [31] U. Schollwöck, *Rev. Mod. Phys.* **77**, 259 (2005).
- [32] G. K.-L. Chan and S. Sharma, *Ann. Rev. Phys. Chem.* **62**, 465 (2011).
- [33] A. R. Edmonds, *Angular Momentum in Quantum Mechanics* (Oxford University Press, USA, 1994), 3rd ed.
- [34] D. M. Brink and G. R. Satchler, *Angular Momentum* (Princeton University Press, Princeton, New Jersey, 1974), 2nd ed.
- [35] T. Xiang, *Phys. Rev. B* **53**, 10445 (1996).
- [36] G. K. L. Chan, *J. Chem. Phys.* **120**, 3172 (2004).
- [37] L. Banci, I. Bertini, G. Gori Savellini, and C. Luchinat, *Inorganic Chemistry* **35**, 4248 (1996).
- [38] O. Hubner and J. Sauer, *Phys. Chem. Chem. Phys.* **4**, 5234 (2002).
- [39] P. Celani, H. Stoll, H.-J. Werner, and P. Knowles, *Mol. Phys.* **102**, 2369 (2004).
- [40] K. Andersson, B. O. Roos, P. A. Malmqvist, and P. O. Widmark, *Chem. Phys. Lett.* **230**, 391 (1994).
- [41] A. O. Mitrushenkov and P. Palmieri, *Chem. Phys. Lett.* **278**, 285 (1997).
- [42] W. J. Hehre, R. F. Stewart, and J. A. Pople, *J. Chem. Phys.* **51**, 2657 (1969).
- [43] A. Becke, *J. Chem. Phys.* **98**, 5648 (1993).
- [44] C. Lee, W. Yang, and R. G. Parr, *Phys. Rev. B* **37**, 785 (1988).
- [45] F. Neese, *Orca version 2.8.0, an ab initio, dft and semiempirical scf-mo package*.
- [46] Y. Kurashige and Y. Takeshi, *J. Phys. Chem.* (2011), submitted.
- [47] S. Östlund and S. Rommer, *Phys. Rev. Lett.* **75**, 3537 (1995).
- [48] U. Schollwöck, *Ann. Phys.* **326**, 96 (2011).

Appendix A: Blocking

In this section we give the formulae for formation of operators R , P and Q in the blocking step of non-spin-adapted and spin-adapted DMRG.

1. Non-spin-adapted DMRG

$$\begin{aligned}
\mathbf{R}_i[\mathcal{A}] = & \mathbf{R}_i[\mathcal{L}] \otimes \mathbf{1}[\bullet_l] + \mathbf{R}_i[\bullet_l] \otimes \mathbf{1}[\mathcal{L}] \\
& + \sum_{j \in \bullet_l} 2\mathbf{P}_{ij}[\mathcal{L}] \otimes \mathbf{a}_j^\dagger[\bullet_l] + \mathbf{Q}_{ij}[\mathcal{L}] \otimes \mathbf{a}_i[\bullet_l] \\
& + \sum_{j \in \mathcal{L}} 2\mathbf{P}_{ij}[\bullet_l] \otimes \mathbf{a}_j^\dagger[\mathcal{L}] + \mathbf{Q}_{ij}[\bullet_l] \otimes \mathbf{a}_i[\mathcal{L}]
\end{aligned} \tag{A1}$$

$$\begin{aligned}
\mathbf{Q}_{ij}[\mathcal{A}] = & \mathbf{Q}_{ij}[\mathcal{L}] \otimes \mathbf{1}[\bullet_l] + \mathbf{Q}_{ij}[\bullet_l] \otimes \mathbf{1}[\mathcal{L}] \\
& + 2 \sum_{\substack{k \in \bullet_l \\ l \in \mathcal{L}}} \left((v_{ikjl} - v_{iklj}) \mathbf{a}_k^\dagger[\bullet_l] \otimes \mathbf{a}_l[\mathcal{L}] \right. \\
& \left. + (v_{iljk} - v_{ilkj}) \mathbf{a}_k[\bullet_l] \otimes \mathbf{a}_l^\dagger[\mathcal{L}] \right)
\end{aligned} \tag{A2}$$

$$\begin{aligned}
\mathbf{P}_{ij}[\mathcal{A}] = & \mathbf{P}_{ij}[\mathcal{L}] \otimes \mathbf{1}[\bullet_l] + \mathbf{P}_{ij}[\bullet_l] \otimes \mathbf{1}[\mathcal{L}] \\
& + \sum_{\substack{k \in \bullet_l \\ l \in \mathcal{L}}} (v_{ijlk} \mathbf{a}_k[\bullet_l] \otimes \mathbf{a}_l[\mathcal{L}] + v_{ijkl} \mathbf{a}_k[\bullet_l] \otimes \mathbf{a}_l[\mathcal{L}])
\end{aligned} \tag{A3}$$

2. Spin-adapted DMRG

$$\begin{aligned}
\mathbf{R}_i^{1/2}[\mathcal{A}] = & \mathbf{R}_i^{1/2}[\mathcal{L}] \otimes_{1/2} \mathbf{1}^0[\bullet_l] + \mathbf{R}_i^{1/2}[\bullet_l] \otimes_{1/2} \mathbf{1}^0[\mathcal{L}] \\
& + \sum_{j \in \bullet_l} \frac{\sqrt{3}}{2} \mathbf{P}_{ji}^1[\mathcal{L}] \otimes_{1/2} \mathbf{a}_j^{1/2}[\bullet_l] + \frac{1}{2} \mathbf{P}_{ji}^0[\mathcal{L}] \otimes_{1/2} \mathbf{a}_i^{1/2}[\bullet_l] \\
& + \sum_{j \in \bullet_l} \frac{\sqrt{3}}{2} \mathbf{Q}_{ij}^{1\dagger}[\mathcal{L}] \otimes_{1/2} \mathbf{a}_j^{1/2\dagger}[\bullet_l] - \frac{1}{2} \mathbf{Q}_{ij}^{0\dagger}[\mathcal{L}] \otimes_{1/2} \mathbf{a}_i^{1/2\dagger}[\bullet_l] \\
& + \sum_{j \in \mathcal{L}} \frac{\sqrt{3}}{2} \mathbf{P}_{ji}^1[\bullet_l] \otimes_{1/2} \mathbf{a}_j^{1/2}[\mathcal{L}] + \frac{1}{2} \mathbf{P}_{ji}^0[\bullet_l] \otimes_{1/2} \mathbf{a}_i^{1/2}[\mathcal{L}] \\
& + \sum_{j \in \mathcal{L}} \frac{\sqrt{3}}{2} \mathbf{Q}_{ij}^{1\dagger}[\bullet_l] \otimes_{1/2} \mathbf{a}_j^{1/2\dagger}[\mathcal{L}] - \frac{1}{2} \mathbf{Q}_{ij}^{0\dagger}[\bullet_l] \otimes_{1/2} \mathbf{a}_i^{1/2\dagger}[\mathcal{L}]
\end{aligned} \tag{A4}$$

$$\begin{aligned}
\mathbf{Q}_{ij}^1[\mathcal{A}] = & \mathbf{Q}_{ij}^1[\mathcal{L}] \otimes_1 \mathbf{1}^0[\bullet_l] + \mathbf{Q}_{ij}^1[\bullet_l] \otimes_1 \mathbf{1}^0[\mathcal{L}] \\
& - \sum_{\substack{l \in \bullet_l \\ k \in \mathcal{L}}} \left(v_{kijl} \mathbf{a}_l^{1/2;\dagger}[\bullet_l] \otimes_1 \mathbf{a}_k^{1/2}[\mathcal{L}] \right. \\
& \left. + v_{ljk} \mathbf{a}_l^{1/2}[\bullet_l] \otimes_1 \mathbf{a}_k^{1/2\dagger}[\mathcal{L}] \right)
\end{aligned} \tag{A5}$$

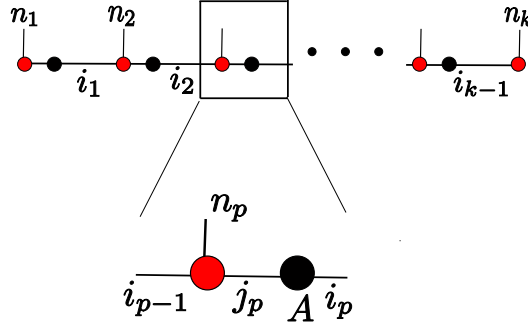


FIG. 4: The figure shows the graphical representation of the MPS wavefunction that can be obtained using the results of the spin-adpated DMRG calculation. The red dots represent a matrix of Clebsch-Gordan coefficients (\mathbf{U}^n) and the black dots are the rotation matrices obtained from the renormalization step in DMRG (\mathbf{L}, \mathbf{R} see text for details).

$$\begin{aligned} \mathbf{Q}_{ij}^0[\mathcal{A}] &= \mathbf{Q}_{ij}^0[\mathcal{L}] \otimes_0 \mathbf{1}^0[\bullet_l] + \mathbf{Q}_{ij}^0[\bullet_l] \otimes_0 \mathbf{1}^0[\mathcal{L}] \\ &- \sum_{\substack{l \in \bullet_l \\ k \in \mathcal{L}}} \left((2v_{ikjl} - v_{kijl}) \mathbf{a}_l^{1/2; \dagger}[\bullet_l] \otimes_0 \mathbf{a}_k^{1/2}[\mathcal{L}] \right. \\ &\quad \left. + (2v_{iljk} - v_{lijk}) \mathbf{a}_l^{1/2}[\bullet_l] \otimes_0 \mathbf{a}_l^{1/2 \dagger}[\mathcal{L}] \right) \end{aligned} \quad (\text{A6})$$

$$\begin{aligned} \mathbf{P}_{ij}^1[\mathcal{A}] &= \mathbf{P}_{ij}^1[\mathcal{L}] \otimes_1 \mathbf{1}^0[\bullet_l] + \mathbf{P}_{ij}^1[\bullet_l] \otimes_1 \mathbf{1}^0[\mathcal{L}] \\ &- \sum_{\substack{k \in \mathcal{L} \\ l \in \bullet_l}} v_{ijlk} \mathbf{a}_k^{1/2 \dagger}[\bullet_l] \otimes_1 \mathbf{a}_l^{1/2 \dagger}[\mathcal{L}] \end{aligned} \quad (\text{A7})$$

$$\begin{aligned} \mathbf{P}_{ij}^0[\mathcal{A}] &= \mathbf{P}_{ij}^0[\mathcal{L}] \otimes_1 \mathbf{1}^0[\bullet_l] + \mathbf{P}_{ij}^0[\bullet_l] \otimes_1 \mathbf{1}^0[\mathcal{L}] \\ &+ \sum_{\substack{k \in \mathcal{L} \\ l \in \bullet_l}} (v_{ijlk} - v_{ijkl}) \mathbf{a}_k^{1/2 \dagger}[\bullet_l] \otimes_0 \mathbf{a}_l^{1/2 \dagger}[\mathcal{L}] \end{aligned} \quad (\text{A8})$$

Appendix B: Matrix Product State formulation

The wavefunction emerging from the usual non-spin-adapted DMRG has a matrix product state (MPS) structure as described in many references [32, 47, 48]. In the canonical form associated with a given block configuration, the MPS wavefunction is written as (using the one-dot formulation of the DMRG for simplicity [47, 48])

$$|\Psi\rangle = \sum_{\{\mathbf{n}\}} \mathbf{L}^{n_1} \mathbf{L}^{n_2} \dots \mathbf{C}^{n_p} \mathbf{R}^{n_{p+1}} \dots \mathbf{R}^{n_k} |\mathbf{n}\rangle \quad (\text{B1})$$

where $|\mathbf{n}\rangle$ denotes a Slater determinant in occupation number representation, \mathbf{L}^n is a left transformation matrix as defined in Eq. (10), obtained during the forwards DMRG sweep, \mathbf{R}^n is a right transformation matrix, obtained during the backwards sweep, and \mathbf{C}^{n_p} is the wavefunction coefficient matrix.

In the case of the spin-adapted DMRG, the wavefunction also has a matrix product state form. However, the transformation matrices \mathbf{L}^n , \mathbf{R}^n now assume a special restricted structure. In particular,

$$\mathbf{L}^n = \mathbf{U}^n \underline{\mathbf{L}} \quad (\text{B2})$$

$$\mathbf{R}^n = \underline{\mathbf{R}} \mathbf{U}^n \quad (\text{B3})$$

Here \mathbf{U}^n is a unitary matrix containing the Clebsch-Gordan coefficients that construct pure spin states out of the product states $|l\rangle|n_l\rangle$, $|n_r\rangle|r\rangle$, and \mathbf{L} , \mathbf{R} are transformation matrices that map from the complete basis of pure spin states to the renormalised spin state basis. In addition, \mathbf{L} and \mathbf{R} also display a special block structure, namely states with different spins are not mixed. Overall, we can view the spin-adapted DMRG algorithm as carrying out an energy minimization within the space of matrix product states, subject to the above restrictions.

Appendix C: $3j$ coefficients

The Clebsch-Gordan coefficients are related to the Wigner $3j$ symbols as shown below.

$$c_{m_2 m m_1}^{S_2 S S_1} = (-1)^{S_2 - S + m_2} (2S_1 + 1)^{1/2} \begin{pmatrix} S_2 & S & S_1 \\ m_2 & m & -m_1 \end{pmatrix} \quad (\text{C1})$$

The Wigner $3j$ coefficients have some convenient symmetry properties. Two which we make use of are

$$\begin{pmatrix} j_1 & j_2 & j_3 \\ \mu_1 & \mu_2 & \mu_3 \end{pmatrix} = (-1)^{j_1 + j_2 + j_3} \begin{pmatrix} j_2 & j_1 & j_3 \\ \mu_2 & \mu_1 & \mu_3 \end{pmatrix} \quad (\text{C2})$$

$$\begin{pmatrix} j_1 & j_2 & j_3 \\ \mu_1 & \mu_2 & \mu_3 \end{pmatrix} = (-1)^{j_1 + j_2 + j_3} \begin{pmatrix} j_1 & j_2 & j_3 \\ -\mu_1 & -\mu_2 & -\mu_3 \end{pmatrix} \quad (\text{C3})$$

1. Adjoint of operator

The reduced matrix elements of the adjoint of a tensor operator is not the same as the adjoint of the reduced matrix elements of the tensor operator. The reduced matrix elements of the adjoint of tensor operators appearing in our spin-adapted DMRG implementation are shown below,

$$\langle \mu' j || O^{0\dagger} || \mu j \rangle = \langle \mu j || O^0 || \mu' j \rangle \quad (\text{C4})$$

$$\langle \mu' j || O^{1\dagger} || \mu j \rangle = \langle \mu j || O^1 || \mu' j \rangle \quad (\text{C5})$$

$$\langle \mu j + 1 || O^{1\dagger} || \mu' j \rangle = (-1) \sqrt{\frac{2j+3}{2j+1}} \langle \mu' j || O^1 || \mu j + 1 \rangle \quad (\text{C6})$$

$$\langle \mu j + \frac{1}{2} || O^{1/2\dagger} || \mu' j \rangle = \sqrt{\frac{2j+2}{2j+1}} \langle \mu' j || O^{1/2} || \mu j + \frac{1}{2} \rangle \quad (\text{C7})$$

Here we only derive Eq. (C7) and the other equations can be derived in an analogous fashion. Of course one has to remember that the adjoint here is defined as in Eq. (30) and in derivation below T is the adjoint of O . In the derivation below the first equation is valid because the Clebsch-Gordan coefficient is non-zero. In fact this Clebsch-Gordan coefficient is always equal to 1.

$$\begin{aligned}
\langle \mu j + \frac{1}{2} || T^{1/2} || \mu' j \rangle &= C_{j, \frac{1}{2}, j + \frac{1}{2}}^{j, \frac{1}{2}, j + \frac{1}{2}} \langle \mu j + \frac{1}{2} j + \frac{1}{2} | T^{1/2, 1/2} | \mu' j j \rangle \\
&= (2j+1)^{1/2} \begin{pmatrix} j & \frac{1}{2} & j + \frac{1}{2} \\ j & \frac{1}{2} & -j - \frac{1}{2} \end{pmatrix} \langle \mu' j j | T^{1/2, 1/2 \dagger} | \mu j + \frac{1}{2} j + \frac{1}{2} \rangle \\
&= (2j+2)^{1/2} (-1)^{2j+1} \begin{pmatrix} j + \frac{1}{2} & \frac{1}{2} & j \\ -j - \frac{1}{2} & \frac{1}{2} & j \end{pmatrix} \langle \mu' j j | -O^{1/2, -1/2} | \mu j + \frac{1}{2} j + \frac{1}{2} \rangle \\
&= - (2j+2)^{1/2} \begin{pmatrix} j + \frac{1}{2} & \frac{1}{2} & j \\ j + \frac{1}{2} & -\frac{1}{2} & -j \end{pmatrix} \langle \mu' j j | O^{1/2, -1/2} | \mu j + \frac{1}{2} j + \frac{1}{2} \rangle \\
&= - \sqrt{\frac{2j+2}{2j+1}} (2j+1)^{1/2} \begin{pmatrix} j + \frac{1}{2} & \frac{1}{2} & j \\ j + \frac{1}{2} & -\frac{1}{2} & -j \end{pmatrix} \langle \mu' j j | O^{1/2, -1/2} | \mu j + \frac{1}{2} j + \frac{1}{2} \rangle \\
&= - \sqrt{\frac{2j+2}{2j+1}} C_{j + \frac{1}{2}, -\frac{1}{2}, j}^{j + \frac{1}{2}, \frac{1}{2}, j} \langle \mu' j j | O^{1/2, -1/2} | \mu j + \frac{1}{2} j + \frac{1}{2} \rangle \\
&= - \sqrt{\frac{2j+2}{2j+1}} \langle \mu' j || O^{1/2} || \mu j + \frac{1}{2} \rangle
\end{aligned} \tag{C8}$$